# Hyperpolarizability Effects in a Sr Optical Lattice Clock

Anders Brusch, Rodolphe Le Targat, Xavier Baillard, Mathilde Fouché, and Pierre Lemonde*

*LNE-SYRTE, Observatoire de Paris, 61, Avenue de l'Observatoire, 75014 Paris, France*

(Received 21 December 2005; published 16 March 2006)

We report the observation of a higher-order frequency shift due to the trapping field in a $^{87}$Sr optical lattice clock. We show that, at the magic wavelength of the lattice, where the first-order term cancels, the higher-order shift will not constitute a limitation to the fractional accuracy of the clock at a level of $10^{-18}$. This result is achieved by operating the clock at very high trapping intensity up to 400 kW/cm$^2$ and by a specific study of the effect of the two two-photon transitions near the magic wavelength.

DOI: 10.1103/PhysRevLett.96.103003 PACS numbers: 32.80.−t, 06.30.Ft, 42.50.Hz, 42.62.Fi

Cold atoms confined in optical lattices have become tools of growing importance to several fields in physics such as quantum computing [1], matter wave manipulation [2], cavity QED [3,4], or precision measurements [5–9]. Examples of their interesting features are long quantum coherence times, controllable collisions, controllable position of the atoms, and Lamb-Dicke confinement. All the related experiments share the same need for a constantly improved control of the atom-lattice interaction. For instance, trapping a single atom in a high-$Q$ cavity in the strong coupling regime has been achieved by adjusting the trap parameters to make the potential "state insensitive" [3]. In another experiment, the lifetime of the quantum coherences of atomic qubits is limited by the fluctuations of the differential light shift due to the lattice [10]. The energy shift of the atomic levels induced by the relatively strong lattice field is a topical problem and is the subject of this Letter.

The challenge is easily understood in the case of atomic clocks, which are more specifically studied here. In this domain, the recent proposal [11] and preliminary realizations [7–9] of optical lattice clocks open a promising route towards frequency standards with a fractional accuracy better than $10^{-17}$. A large number of atoms are confined in the Lamb-Dicke regime, which, in principle, allows both the high signal to noise ratio of optical clocks with neutral atoms [12] and the cancellation of motional effects of trapped ion devices [13–16]. For an optical lattice clock with Sr atoms, the typical requirement in terms of trapping depth is about $10E_r$, with $E_r$ the recoil energy associated to the absorption of a lattice photon [17]. The corresponding frequency shift of both clock states amounts to 36 kHz at 800 nm, while a relative accuracy goal of $10^{-18}$ implies a control of the differential shift at the 0.5 mHz level, or $10^{-8}$ in fractional units.

The frequency of the clock transition in a lattice of depth $U_0$ is shifted with respect to the unperturbed frequency $\nu_0$ according to

$$\nu = \nu_0 + \nu_1 \frac{U_0}{E_r} + \nu_2 \frac{U_0^2}{E_r^2} + O\left(\frac{U_0^3}{E_r^3}\right), \qquad (1)$$

with $\nu_1$ and $\nu_2$ proportional to the (dynamic) polarizability and hyperpolarizability difference between both states of the clock transition [11]. By the principle of the optical lattice clock, $\nu_1$ cancels when the trapping laser is tuned to the "magic wavelength" $\lambda_m$. Although this remains to be demonstrated experimentally, a control of this first-order frequency shift to better than 1 mHz seems achievable [11].

The higher-order term is *a priori* more problematic with no expected cancellation. A theoretical calculation of the effect is reported in Ref. [11], predicting a frequency shift of $-2$ $\mu$Hz$/E_r^2$ for a linear polarization of the lattice. The calculation, however, was performed at the theoretical magic wavelength of 800 nm. The actual value [18] $\lambda_m =$ 813.428(1) nm (see [7,9] and below) lies near two two-photon resonances which may considerably enhance the effect and impede the realization of an accurate clock. The first one couples $5s5p\,^3P_0$ to $5s7p\,^1P_1$ (Fig. 1) and is at a wavelength of 813.36 nm or, equivalently, 30 GHz away from the magic wavelength. Although this $J = 0 \rightarrow J = 1$ two-photon transition is forbidden to leading order for two photons of identical frequencies [19], it is so close to the magic wavelength that it has to be *a priori* considered. The second one resonantly couples $5s5p\,^3P_0$ to $5s4f\,^3F_2$ at 818.57 nm and is fully allowed.

We report here an experimental study of higher-order effects in a $^{87}$Sr optical lattice clock operating at a very high trapping depth up to $1400E_r$ and for a linear polar-

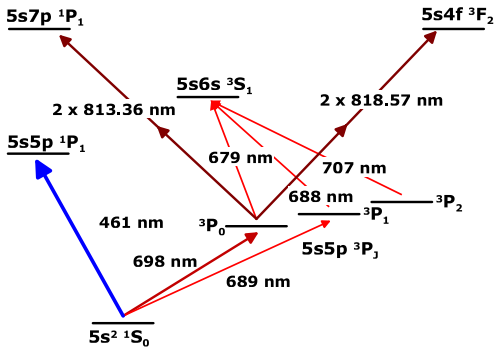


FIG. 1 (color online). Energy levels of Sr relevant to this Letter. The clock transition at 698 nm couples the two lowest energy states of the atom.

 

ization of the lattice. This depth is about a factor of 10 higher than in the other reported systems [7,9] which enhances the sensitivity to higher-order frequency shifts by 2 orders of magnitude. The high trapping depth is reached thanks to an enhancement Fabry-Pérot cavity around the 1D vertical lattice. The circulating power reaches 16 W for a 650 mW input at 813 nm. The mode has a waist radius of 90 $\mu$m corresponding to a maximum $U_0 = 1400E_r$ and an axial (radial) oscillation frequency of 260 kHz (540 Hz). An intracavity dichroic mirror separates the lattice light from that which probes the clock transition. It induces negligible intracavity loss at 813 nm while ensuring that less than $10^{-3}$ of the incident power at 698 nm is reflected back to the atoms by the cavity mirror. The lattice polarization is interferometrically filtered by an intracavity quarter wave plate, which lifts the degeneracy between the linear polarization states parallel to the eigenaxis of the plate by half a free spectral range. The resulting polarization of the trapping light is linear to better than $10^{-3}$. Its wavelength $\lambda_L$ is controlled by means of a wave meter with an accuracy of $10^{-3}$ nm.

Atoms are loaded into the optical lattice from the magneto-optical trap (MOT) described in Ref. [20]. Throughout the loading cycle, the lattice is overlapped with the MOT. Cold atoms at the center of the trap are selectively optically pumped to the metastable $^3P_{0,2}$ states by means of two ''drain'' lasers of waist radius 50 $\mu$m that are aligned to the lattice. They are tuned to the $^1S_0 - {}^3P_1$ and $^3P_1 - {}^3S_1$ transitions at 689 and 688 nm, respectively (Fig. 1). Atoms in the metastable states remain trapped provided their energy is smaller than the 200 $\mu$K lattice depth. This leads to a continuous loading of the lattice at a rate of about $10^5$ atoms/s. After half a second of loading time, the MOT and drain lasers are switched off, and the atoms are repumped back to the ground state using two lasers tuned to the $^3P_{0,2} - {}^3S_1$ transitions at 679 and 707 nm. They are then cooled in the lattice to $\sim$10 $\mu$K in 50 ms with the narrow $^1S_0 - {}^3P_1$ intercombination line at 689 nm [21].

Following this preparation stage, we probe the $^1S_0 - {}^3P_0$ clock transition at 698 nm. The frequency of the probe laser is referenced to an ultrastable cavity as described in Ref. [22]. The probe beam is aligned parallel to the lattice and has a waist radius of 200 $\mu$m. Its polarization is linear and parallel to the lattice polarization. After the probe pulse, the transition probability to $^3P_0$ is measured in a few milliseconds by laser-induced fluorescence. A first detection pulse at 461 nm gives the number of atoms remaining in the ground state and ejects these atoms from the trap. Atoms in $^3P_0$ are then repumped to the ground state with the 679 and 707 nm lasers and detected similarly. This method allows a transition probability measurement which is insensitive to the atom number fluctuations. The resonance is shown in Fig. 2. The central feature (the carrier) is zoomed in the inset in the figure. Its linewidth is 260 Hz in optimal operating conditions: $\lambda_L = \lambda_m$,

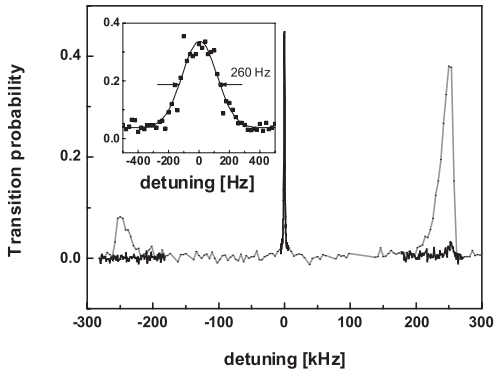


FIG. 2. Motional spectrum of the atoms in the optical lattice. Each point corresponds to a single measurement of 1 s total duration. Black curve: Optimal operating conditions (probe pulse of 10 ms duration and 2 $\mu$W power). The inset is a zoom on the carrier. Grey curve: The first-order longitudinal motional sidebands are enhanced by applying long probe pulses of 200 ms at the maximum available power at 698 nm (2 mW).

probe pulse of 10 ms duration, and 2 $\mu$W power. The resonance plotted here was obtained at the maximum trapping depth, and we observed no clear dependence of its width and contrast with $U_0$. The present limitation to the width of the resonance is probably of technical origin, since linewidths in the 10 Hz range have already been observed in optical lattice clocks [7,8].

The carrier is surrounded by motional sidebands shifted by the oscillation frequency along the lattice direction. They are hardly visible in optimal operation but can be enhanced by applying long pulses of 200 ms duration at the maximum available power (2 mW) of the probe beam. The resulting spectrum is plotted in gray in Fig. 2. The 1:5 ratio between the red and blue sidebands show that 80% of the atoms populate the $|n_z = 0\rangle$ motional state along the lattice axis, corresponding to a temperature of 8 $\mu$K. The transverse temperature is 10 $\mu$K.

The effect of the trap on the clock transition is measured by locking the frequency of the probe laser to the carrier for various values of $U_0$ and $\lambda_L$. The trap depth $U_0$ is adjusted to its desired value between $200E_r$ and $1400E_r$ by a linear ramp of 1 ms duration between the cooling and probing phases. This slightly decreases the transverse temperature while the longitudinal motion is adiabatically cooled by following the ramp. To lock the probe laser frequency, we alternatively probe both sides of the resonance and compute an error signal from the difference between two successive measurements of the transition probability. This also gives a measurement of the difference between the atomic transition and the reference cavity frequency which slowly fluctuates due to thermal effects. These fluctuations behave essentially as a sine wave of peak to peak amplitude 300 Hz and period 10 minutes. To derive the frequency shift due to the lattice, we reject the cavity frequency fluctuations by a factor 100 by a differential method [23]. We interleave measurements at 4 different

lattice depths. We run the clock for 19 cycles before $U_0$ is changed to the next of the four interleaved values. The entire sequence is repeated typically 16 times. The cavity fluctuations are then modeled as a polynomial which is determined by a least-squares fit of the data [24]. The data are corrected for the modeled cavity frequency fluctuations and averaged. This yields 4 statistically independent measurements [25] of the clock transition frequency versus $U_0$ with a standard deviation of about 5 Hz. A typical set of such points is shown in Fig. 3(a).

We perform a quadratic least-squares fit of each set of four points which gives a measurement of the coefficients $\nu_1$ and $\nu_2$ of Eq. (1). The coefficient $\nu_2$ is plotted in Fig. 3(c) and found compatible with zero for the whole range [813.3, 813.5 nm] to within a few tens of microhertz. An especially interesting wavelength region is around 813.36 nm, where the $^3P_0 \rightarrow {}^1P_1$ two-photon transition is expected. The contribution of a two-photon transition to $\nu_2$ varies as $\Delta^{-1}$, with $\Delta$ the detuning of the lattice with respect to the resonance. We magnify this contribution by systematically spanning a frequency range of $\pm 5$ GHz with a 1 GHz step around the expected value [Fig. 3(c)]. The null results of all these measurements demonstrate that the higher-order shift due to the $^3P_0 \rightarrow {}^1P_1$ transition is less than 1 $\mu\text{Hz}/E_r^2$ for $\lambda_L = \lambda_m$. Despite its proximity to the magic wavelength, this two-photon transition is forbidden enough to not be a problem.

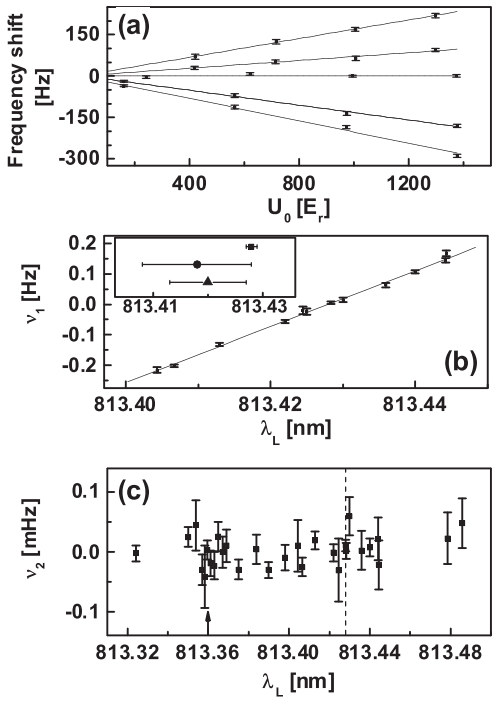


FIG. 3. (a) Typical experimental data used to derive the first- and second-order frequency shift coefficients plotted in (b) and (c). Shown here is the frequency shift of the clock transition vs lattice depth for 5 different lattice wavelengths: 813.406 (four lowest points in the graph), 813.413, 813.428, 813.436, and 813.444 nm (four highest points). Also shown is a linear fit of each of these five sets of data. (b) First-order frequency shift vs $\lambda_L$ scaled back to $U_0 = E_r$. Also plotted is a linear fit of these data ($\chi^2 = 1.1$). The inset shows measurements of $\lambda_m$. ■: this work. ▲: Ref. [7]. ●: Ref. [9]. (c) Higher-order frequency shift vs $\lambda_L$ scaled back to $U_0 = E_r$. All these points are compatible with zero. Their average is $-4(36) \times 10^{-7}$ Hz ($\chi^2 = 1.02$). The arrow on the $\lambda_L$ axis corresponds to the $^3P_0 \rightarrow {}^1P_1$ transition at 813.360 nm. The vertical dotted line is at the magic wavelength 813.428 nm.

This set of experiments around 813.4 nm can also be used to derive an accurate value of $\lambda_m$. Having shown that $\nu_2$ is negligible for $\lambda_L \sim \lambda_m$, better estimates of $\nu_1$ are obtained with linear fits of each set of four points. They are plotted in Fig. 3(b). We find $\lambda_m = 813.428(1)$ nm in agreement with previously published values [7,9] as shown in the inset in Fig. 3(b). The improvement by one order of the accuracy of this measurement is a nice illustration of the amplification of the effects of the lattice offered by a deep trapping potential.

We also studied the effect of the other two-photon transition in this wavelength region, the $^3P_0 \rightarrow {}^3F_2$ at 818.57 nm. When tuned 5 nm away from $\lambda_m$, we expect, in addition to the effect of the two-photon coupling, a trivial quadratic dependence of the atomic frequency vs $U_0$ due to the imperfect cancellation of $\nu_1$ and to the inhomogeneity of the laser intensity experienced by the atoms. We do observe a substantial broadening and asymmetry of the resonance due to this effect similar to what was reported in Ref. [26]. The associated trivial quadratic frequency shift amounts to 0.8 $\text{mHz}/E_r^2$ as measured several gigahertz away on both sides of the two-photon transition.

When tuned closer to the resonance, we clearly observe the nontrivial quadratic frequency shift due to the two-photon resonance itself. The effect is shown in Fig. 4. Quadratic frequency shifts of several kilohertz and changing sign, depending on the side of the transition being probed are observed, as shown in Fig. 4(b). This is a clear signature of the higher-order effects due to the particular transition under investigation. When tuned exactly onto one of the five transitions corresponding to the hyperfine structure of $^3F_2$, the lattice laser induces severe loss (up to 90%) of atoms when the 698 nm probe laser is tuned to resonance. This effect, which we attribute to three-photon ionization from $^3P_0$, was used to determine the position of the five hyperfine substates shown by arrows in Fig. 4(a). The hyperfine structure of $^3F_2$ leads to a complex dependence of the quadratic frequency shift on the lattice wavelength around resonance. The contribution of the five substates can interfere with each other, which may be the cause of the oscillations of $\nu_2$ seen in Fig. 4(a) on both sides of the hyperfine manifold. We can deduce from our measurements a conservative estimate of the contribution of the $^3P_0 - {}^3F_2$ resonance to the higher-order effects at $\lambda_L = \lambda_m$. The gray dashed curve plotted in Fig. 4(a) scales as the inverse of the detuning of the lattice with respect to the center of gravity of the hyperfine structure of $^3F_2$ and

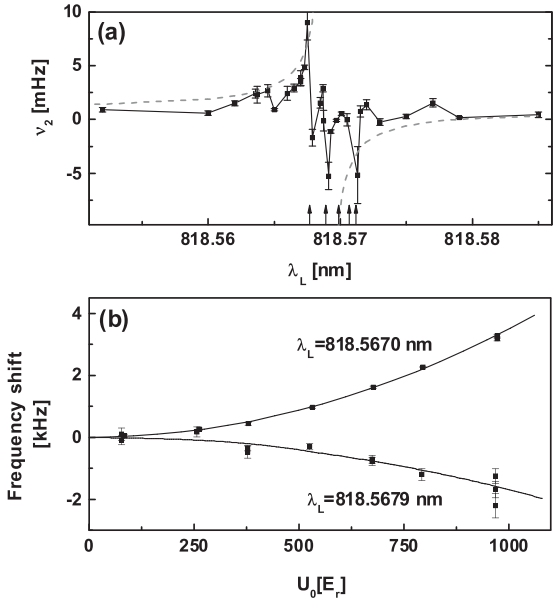


FIG. 4. (a) Higher-order frequency shift around the $^3P_0 \rightarrow {}^3F_2$ transition at 818.570 nm scaled back to $U_0 = E_r$. The five vertical arrows on the wavelength axis correspond to the hyperfine substates of $5s4f\,{}^3F_2$ ($F = 13/2$ to $F = 5/2$ from left to right). (b) Atomic frequency shift vs trapping depth for two lattice wavelengths on both sides of the two-photon transition to substate $F = 13/2$. The linear light shift has been removed for clarity. The bold line is a fit of the data with a parabola.

envelopes experimental points. When extrapolated to the magic wavelength, it gives a contribution to $\nu_2$ of 2 $\mu$Hz or, equivalently, a quadratic frequency shift of 0.2 mHz for a lattice depth of $10E_r$.

Finally, we have performed an extensive series of measurements of the clock frequency as a function of the lattice depth at $\lambda_L = \lambda_m$. The values of $\nu_2$ derived from these measurements are plotted in Fig. 5. Their weighted average gives $\nu_2(\lambda_m) = 7(6)$ $\mu$Hz. For a lattice depth $U_0 = 10E_r$, the corresponding frequency shift is lower than 1 mHz (one sigma) or $2 \times 10^{-18}$ in fractional units. This demonstrates that the frequency shift due to the atomic hyperpolarizability constitutes no impediment to the accuracy of a Sr optical lattice clock down to the $10^{-18}$ level. In addition, the effective laser intensity seen by the atoms is certainly controllable at the percent level [27]. The performance of the system would then be immune to higher-order frequency shifts over a broad lattice depth range, possibly up to $U_0 = 100E_r$. This would provide a powerful lever for the experimental evaluation at the $10^{-18}$ level of other effects associated, for instance, to the dynamics of the atoms in the lattice or to cold collisions. Collisions are expected to be negligible with polarized fermions, but they have to be considered if one uses bosonic isotopes [8], such as $^{88}$Sr. By varying the trapping depth, one can adjust the tunneling rate and then control the overlap of the wave functions of atoms confined in the lattice, allowing the study of cold collisions in a new regime.

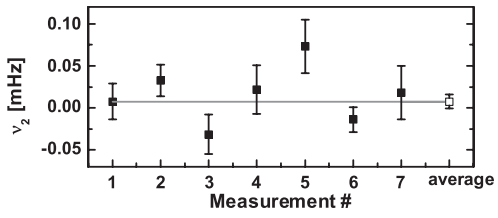


FIG. 5. Higher-order frequency shift at the magic wavelength scaled back to $U_0 = E_r$. The value of the open square is the weighted average of the seven other points ($\chi^2 = 1.8$).

We thank A. Clairon and C. Salomon for useful comments and discussions on the manuscript. SYRTE is Unité Associée au CNRS (UMR 8630) and a member of IFRAF (Institut Francilien de Recherche sur les Atomes Froids). This work is supported by CNES and DGA.

*Electronic address: pierre.lemonde@obspm.fr

[1] J. J. Garcia-Ripoll, P. Zoller, and J. I. Cirac, J. Phys. B **38**, S567 (2005).
[2] I. Bloch, Nature Phys. **1**, 23 (2005).
[3] J. McKeever *et al.*, Phys. Rev. Lett. **90**, 133602 (2003).
[4] S. Nußmann *et al.*, Phys. Rev. Lett. **95**, 173602 (2005).
[5] I. Carusotto *et al.*, Phys. Rev. Lett. **95**, 093202 (2005).
[6] P. Cladé *et al.*, Phys. Rev. Lett. **96**, 033001 (2006).
[7] M. Takamoto, F.-L. Hong, R. Higashi, and H. Katori, Nature (London) **435**, 321 (2005).
[8] Z. W. Barber *et al.*, Phys. Rev. Lett. **96**, 083002 (2006).
[9] A. D. Ludlow *et al.*, Phys. Rev. Lett. **96**, 033003 (2006).
[10] S. Kuhr *et al.*, Phys. Rev. A **72**, 023406 (2005).
[11] H. Katori, M. Takamoto, V. G. Pal'chikov, and V. D. Ovsiannikov, Phys. Rev. Lett. **91**, 173005 (2003).
[12] U. Sterr *et al.*, C.R. Physique **5**, 845 (2004).
[13] H. S. Margolis *et al.*, Science **306**, 1355 (2004).
[14] W. H. Oskay, W. M. Itano, and J. C. Bergquist, Phys. Rev. Lett. **94**, 163001 (2005).
[15] T. Schneider, E. Peik, and C. Tamm, Phys. Rev. Lett. **94**, 230801 (2005).
[16] P. Dubé *et al.*, Phys. Rev. Lett. **95**, 033001 (2005).
[17] P. Lemonde and P. Wolf, Phys. Rev. A **72**, 033409 (2005).
[18] All wavelengths throughout the Letter are in vacuum.
[19] G. Grynberg and B. Cagnac, Rep. Prog. Phys. **40**, 791 (1977).
[20] I. Courtillot *et al.*, Opt. Lett. **28**, 468 (2003).
[21] T. Mukaiyama *et al.*, Phys. Rev. Lett. **90**, 113002 (2003).
[22] A. Quessada *et al.*, J. Opt. B **5**, S150 (2003).
[23] Y. Sortais *et al.*, Phys. Rev. Lett. **85**, 3117 (2000).
[24] We use a tenth-order polynomial fit of the data. For any polynomial order between 5 and 14, the results are unchanged to within a fraction of the error bars.
[25] Except for a common offset which does not play any role in further data analysis.
[26] M. Takamoto and H. Katori, Phys. Rev. Lett. **91**, 223001 (2003).
[27] A control to within a few percent is already achieved in our setup as evidenced by the nice alignment of the measurements of $\nu_1$ shown in Fig. 3(b).